Transition from a weak ferromagnetic insulator to an exchange-enhanced paramagnetic metal in the $BaIrO_3$ polytypes

J.-G. Cheng,[1] J.-S. Zhou,[1,*] J. A. Alonso,[1,2,3] J. B. Goodenough,[1] Y. Sui,[4] K. Matsubayashi,[5] and Y. Uwatoko[5]
[1]*Texas Materials Institute, University of Texas at Austin, Austin, Texas 78712, USA*
[2]*Instituto de Ciencia de Materiales de Madrid, CSIC, Cantoblanco, E-28049 Madrid, Spain*
[3]*Institute Laue-Langevin (ILL), 156X, F-38042 Grenoble Cedex 9, France*
[4]*Center for Condensed Matter Science and Technology, Department of Physics, Harbin Institute of Technology, Harbin 150001, China*
[5]*Institute for Solid State Physics, University of Tokyo, Kashiwa 277-8581, Japan*
(Received 23 July 2009; published 24 September 2009)

As a follow-up of the high-pressure synthesis and the structural determination of two new $BaIrO_3$ polytypes, we report in this paper a systematic study of the physical properties of all polytypes available to us through measurements of magnetic, electronic transport, thermodynamic, and low-temperature structural as well as pressure effects. With increasing fraction of the corner- to face-sharing octahedra in the sequence $9R$ $(hhChhChhC) \rightarrow 5H(hChCC) \rightarrow 6H(hCChCC)$, the ground states of $BaIrO_3$ evolve from a ferromagnetic insulator with $T_c \approx 180$ K in the $9R$ phase to a ferromagnetic metal with $T_c \approx 50$ K in the $5H$ phase, and finally to an exchange-enhanced paramagnetic metal near a quantum critical point (QCP) in the $6H$ phase. The experimental results for the $9R$ phase confirm that the ferromagnetic transition is accompanied by a lattice instability, presumably associated with the formation of a charge density wave. The evidence includes a sudden increase in resistivity and thermoelectric power, an anomaly in the thermal conductivity, an unusual expansion of the c axis, and an extraordinarily large pressure coefficient of T_c. In contrast, the ferromagnetic transition in the $5H$ $BaIrO_3$ only gives rise to weak anomalies in the resistivity and specific heat near T_c, similar to $SrRuO_3$; the $5H$ phase is the first weak ferromagnetic metal among the known oxide iridates. The $6H$ phase remains a paramagnetic metal to the lowest temperature. However, a strongly enhanced thermoelectric power and a non-Fermi-liquid behavior from the resistivity measurement at low temperature show that quantum critical fluctuations play a role in this exchange-enhanced paramagnetic phase. A positive thermoelectric power confirms the charge carriers are holelike for all polytypes, which is consistent with the electronic configuration of Ir(IV) $(5d^5)$ in the low-spin state. The low-temperature specific-heat coefficients and Sommerfeld-Wilson ratios are in agreement with the evolution of the ground states across a ferromagnetic to paramagnetic QCP.

DOI: 10.1103/PhysRevB.80.104430 PACS number(s): 71.30.+h, 72.15.Jf, 75.30.Et

I. INTRODUCTION

Among the $5d$ transition-metal oxides, $BaIrO_3$ is the first known ferromagnetic insulator with $T_c \approx 180$ K.[1] A recent study on a single-crystal sample by Cao *et al.*[2] revealed that the ferromagnetic transition at T_c is accompanied by formation of a charge density wave (CDW). In contrast to localized-spin magnetism,[1] Cao *et al.*[2] proposed a model of band magnetism due to a small exchange splitting with associated CDW below T_c that places a gap at the Fermi surface and induces a subtle lattice distortion at T_c. These arguments, based on measurements on a single-crystal sample, were subsequently supported by a tight-binding band-structure calculation,[3] which showed a sharp peak of the density of states at the Fermi level within its π^* band of t_{2g}-block parentage and partially nested pieces of the Fermi surface. In addition, direct experimental evidence for a small Ir moment comes from a μSR measurement performed by Brooks *et al.*,[4] who observed clear oscillations below T_c and found an extremely small internal field at the muon site, thus ruling out the possibility of a localized-spin configuration. On the other hand, a high-resolution photoemission study on $BaIrO_3$ revealed essentially localized electronic states forming a pseudogap at the Fermi energy E_F for $T > T_c$; below T_c a soft gap opens up at E_F due to the CDW formation.[5] This observation could also explain a semiconductor to insulator transition in the electrical resistivity.[2] The scenario of a simultaneous onset of a CDW and a ferromagnetic transition was recently questioned by Nakano and Terasaki.[6] They carried out similar I-V measurements as in Ref. 2 on their single-crystal $BaIrO_3$ by using a pulsed current in order to exclude the self-heating effects, and they observed the giant nonlinear conduction only below 20 K, well below T_c ~ 180 K. Instead of sliding motion of the CDW, they proposed interplay between two different bands is likely the origin of the nonlinear conduction observed in $BaIrO_3$. Moreover, the critical behavior of the ferromagnetic transition itself is unusual as revealed by the anomalous critical exponents $\beta = 0.82(3)$, $\gamma = 1.03(3)$, and $\delta = 2.20(1)$, which do not belong to any existing universality class.[7] Therefore, the nature of the ferromagnetic transition of $BaIrO_3$ is still under debate.

As shown in Fig. 1(a), the crystal structure of the ambient phase of $BaIrO_3$ consists of Ir_3O_{12} trimers of face-sharing octahedra that are linked by their vertices to form columns parallel to the c axis, with a stacking of layers of corner sharing (C) and face-sharing (h) $IrO_{6/2}$ octahedra in the order $hhChhChhC$ along the c axis. Its space group is monoclinic $C2/m$ and the lattice parameters are $a = 10.0046(3)$ Å, $b = 5.75362(14)$ Å, $c = 15.1839(4)$ Å, and $\beta = 103.27(1)°$. Except for the monoclinic distortion, it is isostructural with the $9R$ $BaRuO_3$. The monoclinic distortion generates twisting

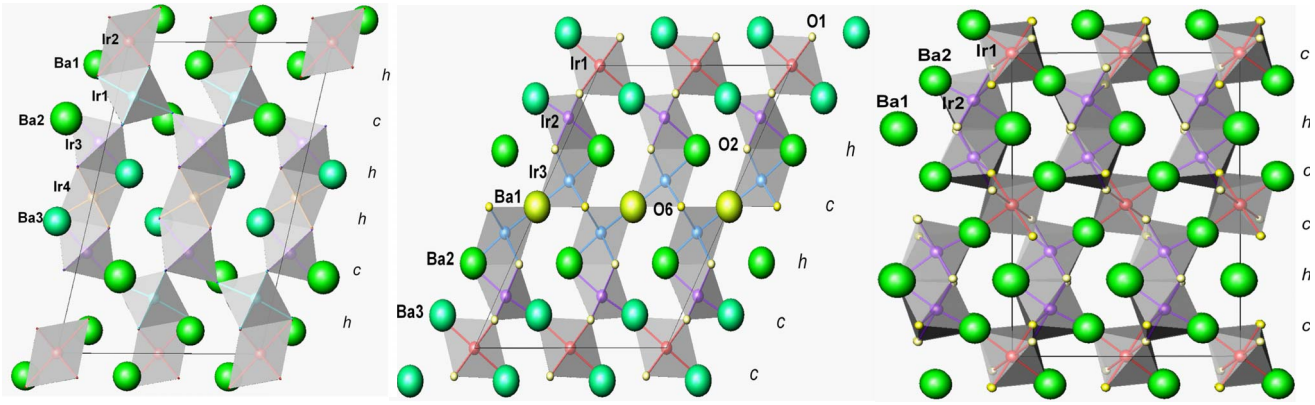

(a) 9R (b) 5H (c) 6H

FIG. 1. (Color online) Crystal structures of $BaIrO_3$ polytypes: (a) 9*R*, (b) 5*H*, and (c) 6*H*.

and buckling of the Ir_3O_{12} trimers that are tilted ~12° relative to each other.

The polytype structures of the ABO_3 oxides and the phase transitions under high pressure were established during the 1960–1970s, see the review.[8] As a general trend, the number of the *h* layer stacking along the *c* axis in a unit cell is reduced as the synthesis pressure increases, which led to the synthesis of a new cubic $BaRuO_3$ under 18 GPa two years ago.[9] The 9*R* $BaRuO_3$ is a paramagnetic metal with an unusual temperature dependence of magnetic susceptibility. A calculation[10] that includes a strong spin-orbit coupling can explain the anomalous $\chi(T)$ to a great extent. The evolution from paramagnetic metal to ferromagnetic metal observed on a series of polytypes 9*R*-4*H*-6*H*-3*C* indicates an increasing bandwidth W that becomes broad enough to suppress the spin-orbit coupling but not eliminate the spin-spin interaction as the population of the *C* layers increases.[9] This work motivated us to explore the evolution of the physical properties of the polytypes of $BaIrO_3$. Starting from the 9*R* phase, we have recently obtained a new member 5*H*, as well as the 6*H* and 3*C* phases of $BaIrO_3$ with high-pressure synthesis.[11] The 5*H* phase can only be synthesized in a very narrow pressure range around 4 GPa. Its crystal structure, shown in Fig. 1(b), contains double Ir_2O_9 dimers of face-sharing octahedra connected by vertices to single $IrO_{6/2}$ octahedra along the *c* axis with a stacking *hChCC*. It is also monoclinic with the space group $C2/m$ and lattice parameters $a=9.9511(2)$ Å, $b=5.7503(1)$ Å, $c=13.71003(3)$ Å, and $\beta=118.404(2)°$. The 6*H* phase can be stabilized between 5 and 10 GPa. The 3*C* phase exists as a minority phase coexisting with the 6*H* in a high-pressure synthesis under 10 GPa.

II. EXPERIMENTAL DETAILS

Details about the sample preparations and structure determination have been published elsewhere.[11] The samples used in this study include: (1) the 9*R* phase prepared under ambient pressure, (2) the 5*H* phase obtained at 4 GPa, and (3) the 6*H* phase obtained at 7.5 GPa. The synthesis at 10 GPa resulted in the product including 95% the 6*H* phase and 5% 3*C* phase as seen from the profile refinement. This sample has been checked only by the thermoelectric power measurement. The dc magnetic susceptibility and magnetization were measured with a commercial superconducting quantum interference device (SQUID) magnetometer (Quantum Design). A four-probe method was used to measure the resistivity. Thermoelectric-power measurements were performed in a home-made setup. The steady-state method was used in our thermal conductivity measurement. The specific-heat measurement was carried out on a physical properties measurement system (PPMS) (Quantum Design) with the two-τ relaxation method. The magnetic susceptibility under high pressure was measured with a miniature Cu-Be cell fitting the SQUID magnetometer. A piece of Pb as the pressure manometer, the sample, and a mixture of 3M Flourinert FC77+FC72 as the pressure medium were sealed in a Teflon capsule. Low-temperature x-ray diffraction (XRD) measurements were carried out in a Schintag theta-theta diffractometer with Cu anode; samples were placed on a cryostat that was cooled down by flowing liquid nitrogen.

III. RESULTS AND DISCUSSIONS

A. Magnetic properties

Figure 2 summarizes the magnetic properties of three $BaIrO_3$ polytypes. The temperature dependence of the dc magnetic susceptibilities $\chi(T)$ were measured with increasing temperature from 5 to 360 K under a magnetic field $H=1$ T after zero-field cooling (ZFC) and field cooling (FC). As shown in Fig. 2(a), the $\chi(T)$ curves of both 9*R* and 5*H* phases exhibit a sharp increase corresponding to a ferromagnetic transition at T_c. From the sharp minimum of the $d\chi/dT$ curves, inset of Fig. 2(a), values of T_c were determined to be 180 and 50 K for the 9*R* and 5*H* phases, respectively. For both phases, the ZFC and FC $\chi(T)$ curves split at a temperature slightly below T_c, which implies the presence of either magnetic frustration or magnetocystalline anisotropy. The nearly similar change of $\chi(T)$ at $T \leq T_c$ found in the 5*H* and 9*R* phases makes the 5*H* phase a new weak ferromagnetic iridate. The observed $T_c=180$ K of the 9*R* phase is in excellent agreement with those reported in the literature.[1,2,6] On the other hand, the 6*H* phase does not show any magnetic

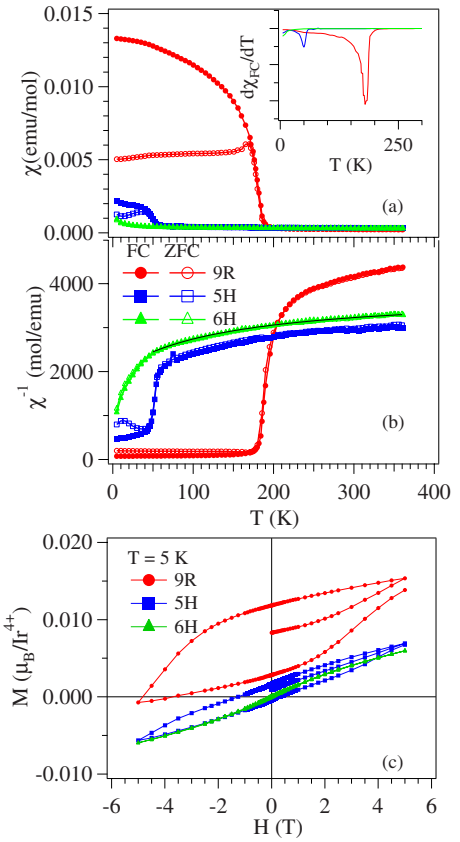

FIG. 2. (Color online) (a) Temperature dependence of the dc magnetic susceptibility χ, (b) χ^{-1}; (c) isothermal magnetization $M(H)$ at 5 K for the three $BaIrO_3$ polytypes. Inset of (a) shows the temperature derivative of the χ_{FC}. Modified Curie-Weiss fitting curves are shown in (b) as the solid lines.

ordering down to 5 K with complete overlapping of the ZFC and FC $\chi(T)$ curves. Thus, with increasing ratio of corner- to face-shared $IrO_{6/2}$ octahedra, the magnetic ordering temperature is reduced dramatically from 180 K in the 9*R* phase to below 5 K in the 6*H* phase. As shown in Fig. 2(b), the $\chi^{-1}(T)$ curves in the paramagnetic region exhibit very weak temperature dependences, suggesting the presence of a large, temperature-independent term, χ_0. Therefore, we have fit the $\chi^{-1}(T)$ in the paramagnetic region with a modified Curie-Weiss (C-W) law, viz., $\chi=\chi_0+C/(T-\theta)$ and extracted the effective paramagnetic moment ($\mu_{\text{eff}}=\sqrt{8C}$) of the Ir(IV) ions and the Weiss temperatures θ. As shown by the solid lines in Fig. 2(b), the fitting is reasonably good. The fitting parameters are given in Table I. The μ_{eff} values increase gradually from 9*R* to 5*H* to 6*H*, but they are much lower than the expected value for the low-spin Ir(IV) with $S=\frac{1}{2}$. A reduced μ_{eff} is commonly observed in most iridates,[2,12,13] and has been attributed to the strong hybridization between iridium 5*d* and oxygen 2*p* orbitals. The χ_0 falls into a narrow range $2.08-2.88\times10^{-4}$ emu/mol Ir(IV) in these three polytypes. The results for the 9*R* phase are consistent with those reported by Cao *et al.*[2] on a single-crystal sample.

Figure 2(c) displays the hysteresis loops, $M(H)$, measured at $T=5$ K after ZFC from 300 K, which indicates that a weak ferromagnetism takes place below T_c in the 9*R* and 5*H* phases. Although the remanent field has been checked and balanced carefully during ZFC, $M(H)$ does not start from the origin as H increases from zero and the coercive field is unusually large. The offset of M at $H=0$ becomes smaller in the 5*H* phase, but it is still visible. On the other hand, any hysteresis loop for the 6*H* phase is negligible and is symmetric about the origin. The magnetic moment per Ir(IV) site at 5 K and 5 T is rather small in all three phases; it increases from 0.006 μ_B (6*H*) to 0.007 μ_B (5*H*) to 0.015 μ_B (9*R*). It has been argued[2] that the small ordered moment of Ir(IV) is due to the *d-p* hybridization and a small exchange splitting rather than a canted-spin in the localized-spin configuration. If the intrinsic *d-p* hybridization is assumed to be the same for the three phases, then the evolution of $M_{5\ \text{K},5\ \text{T}}$ suggests a decreased exchange splitting from the 9*R* to the 6*H* phases. The displaced magnetization curve of the 9*R* phase has also been reported before.[1] The origin of the internal field causing this shift remains unknown.

We note that this band model does not take into consideration the ordering of holes at the face-shared octahedra into *c*-axis orbitals to give three *c*-axis electron/Ir trimer in the 9*R* phase where the Ir-Ir distance is short. With $S=1/2$ per trimer in the 9*R* phase, the ferromagnetic coupling would be between trimers and the moment would be reduced.

TABLE I. Physical properties and fitting parameters of the $BaIrO_3$ polytypes.

		9*R*	5*H*	6*H*
T_c (K)		180(5)	50(3)	
θ_{CW} (K)		162.9(2.8)	−22.3(1.9)	−64.9(3.5)
μ_{eff} (μ_B/Ir)		0.186(6)	0.346(4)	0.364(6)
χ_0 (10^{-4} emu/mol Ir^{4+})		2.08(1)	2.88(1)	2.64(1)
$M_{5\ \text{K},5\ \text{T}}$ (μ_B/Ir^{4+})		0.015(1)	0.007(1)	0.006(1)
$\rho_{300\ \text{K}}$ (mΩ cm)		12.586	6.92	4.07
$\rho_{10\ \text{K}}$ (mΩ cm)		>35000	3.22	1.62
$S_{300\ \text{K}}$ (μV/K)		6.9	5.1	13.6
γ (10^{-3} J/mol K^2)		1.15(8)	6.15(6)	8.99(8)
β (10^{-4} J/mol K^4)		5.04(5)	2.23(4)	1.85(5)
δ (10^{-6} J/mol K^6)		0.95(5)	1.77(4)	1.27(4)
Θ_D (K)		268.2	351.9	374.5
α_a (10^{-5} K^{-1})	$T>T_c$	1.8(1)		
	$T<T_c$	1.2(2)		
α_b (10^{-5} K^{-1})	$T>T_c$	2.3(1)		
	$T<T_c$	1.9(2)		
α_c (10^{-5} K^{-1})	$T>T_c$	0		
	$T<T_c$	−1.9(2)		
α_V (10^{-5} K^{-1})	$T>T_c$	4.1(4)		
	$T<T_c$	1.1(3)		

B. Transport properties

Figure 3 shows the temperature dependence of the resistivity $\rho(T)$ of the $BaIrO_3$ polytypes measured from 8 to 310 K under zero field. The 9*R* phase of Fig. 3(a) is nonmetallic

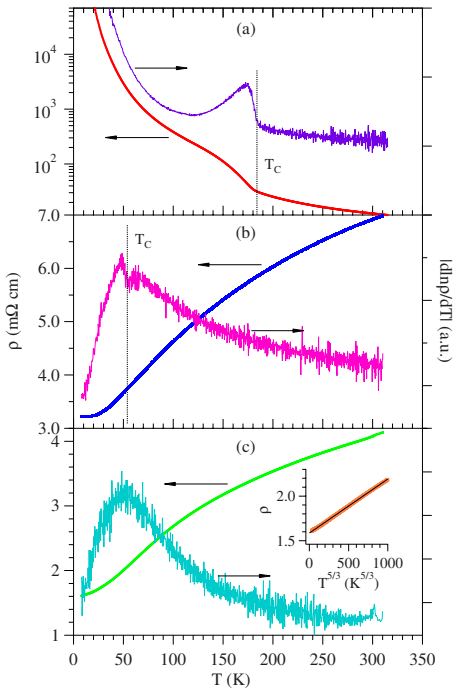

FIG. 3. (Color online) Temperature dependence of the resistivity ρ and its derivative $|d \ln \rho / dT|$ of the $BaIrO_3$ polytypes: (a) 9*R*, (b) 5*H*, and (c) 6*H*. A plot of ρ vs $T^{5/3}$ for the 6*H* $BaIrO_3$ was shown in the inset of (c).

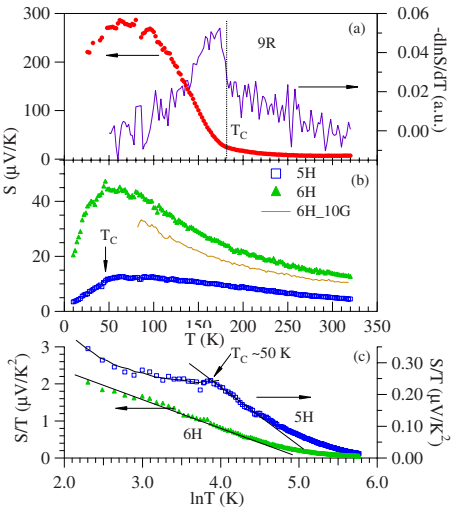

FIG. 4. (Color online) Variation with temperature of the thermoelectric power $S(T)$ for (a) 9*R*, (b) 5*H*, and (c) 6*H* phases. For the 9*R* phase, the ferromagnetic transition T_c can be seen more clearly in the $-d \ln S/dT$ curve. The $S(T)$ data of the 5*H* and 6*H* phases were replotted in the form of S/T vs $\ln T$ in (c).

over the entire temperature range. The ferromagnetic transition causes a sharp anomaly as seen in the derivative $d \ln \rho / dT$. This result is consistent with the opening up of a soft gap at E_F due to the CDW formation as reported previously.[2,5] The weak temperature dependence of $\rho(T)$ at $T > T_c$ does not distinguish whether it is due to a hopping conduction of localized electrons or band conduction with the Fermi energy located in a gap. However, the thermoelectric power at $T > T_c$ in Fig. 4 indicates that there are thermally excited carriers, which suggests that it is a semiconductor with a gap as small as 0.025 eV. The formation of a CDW phase at $T < T_c$ would normally result in a band reconstruction with E_F remaining in the gap if the CDW wavelengths commensurate with the lattice distortion. In this case, a jump of the $S(T)$ at T_c followed by an exponential increase to infinity as T decreases is expected. However, the observed $S(T)$ in Fig. 4(a) peaks out at 70 K. The $S(T)$ at low temperatures behaves like the hopping conduction of small polarons. On the other hand, the structural changes of the polytypes make both the 5*H* and 6*H* metallic. For the 5*H* phase, a weak kink anomaly can be discerned in the $\rho(T)$ of Fig. 3(b) near $T_c \sim 50$ K, which can be seen more clearly from the $d \ln \rho / dT$ curve. Similar to the ferromagnetic transition at T_c in Ni (Ref. 14) or the antiferromagnetic transition at T_N in $Nb_{12}O_{29}$,[15] the anomaly of $\rho(T)$ at the magnetic transition temperature is due to a critical scattering of the conduction electrons from the short-range spin fluctuations. While the phase transition between different polytype structures just quenches the spin-orbit coupling in the $BaRuO_3$ phase with greater *C* stacking, the same structural change enlarges the bandwidth so as to induce the semiconductor-metal transition in the $BaIrO_3$ polytypes. The 5*H* $BaIrO_3$ becomes the first ferromagnetic metal in iridium oxides. As shown in Fig. 3(c), the paramagnetic 6*H* phase is a metal down to 8 K. The structural difference between the 5*H* phase and the 6*H* phase is so small that the ferromagnetic transition should be just suppressed in the 6*H* phase, so a non-Fermi-liquid (NFL) behavior is expected. In order to check out this possibility, we have fit the $\rho(T)$ below $T < 60$ K with a power-law formula $\rho = \rho_{0+} A T^n$, which gives the fitting parameters $\rho_0 = 1.588(1)$ mΩ cm, $A = 5.7(1) \times 10^{-4}$ mΩ cm/$K^{1.68}$, and $n = 1.68(1) \sim 5/3$. A straight line in the ρ vs $T^{5/3}$ plot shown in the inset of Fig. 3(c) confirms the non-Fermi-liquid behavior, which has also been found in systems like $PrNiO_3$ (Ref. 16) and $ZrZn_2$ (Ref. 17) in the vicinity of a quantum critical point (QCP). It is interesting to note that the exponents for the $\rho(T)$ curves of the 6*H* and perovskite $SrIrO_3$ are 3/2 and 2, respectively.[18,19] Therefore, the exponent of 5/3 suggests that the 6*H* phase is located near a QCP between the ferromagnetic metallic state of the 5*H* phase and a Fermi-liquid state of the perovskite phase. Quantum critical fluctuations at low temperatures in the 6*H* phase have been further confirmed by our thermoelectric power measurement in Fig. 4. A superconductive phase has been stabilized at a much lower temperature in some cases in the vicinity of a QCP. We have checked the resistivity of the 6*H* phase down to 0.05 K in an Oxford dilution refrigerator. No superconductive transition was found. However, we did observe an anomalous temperature dependence of resistance in the 5*H* phase within the temperature range of a ^{3}He refrigerator. Figure 3(b) shows a steep resistivity drop at T_c followed by a nearly temperature-independent $\rho(T)$ down to 8 K. This sample was loaded in a high-pressure chamber mounted on an Oxford Heliox probe and measured to 0.355 K under pressure to 16 kbar. As shown in Fig. 5, the resistance undergoes a sharp drop at 3.4 K followed by a semiconductor temperature dependence as temperature further decreases. The transition temperature T_t

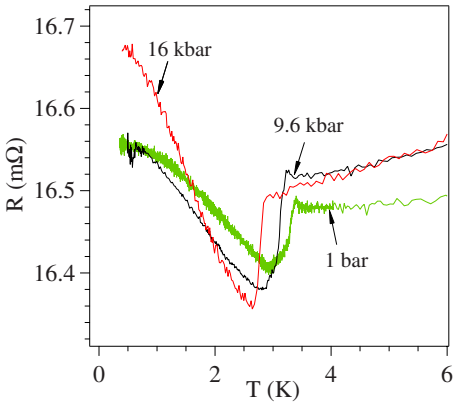

FIG. 5. (Color online) Temperature dependence of the resistance for the 5*H* phase under different pressures. Curves under pressure have been shifted vertically to the level of that at ambient pressure for clarification.

is reduced slightly under pressure; but the resistance drop becomes sharper under pressure. Since no anomaly of the magnetic susceptibility was found, the sharp drop of resistance at T_t is likely caused by superconductive pair fluctuations. The transition to a bulk superconductive phase is truncated by a charge density wave phase at T_t-δT. The origin of this transition deserves further study.

The overall temperature dependence of the thermoelectric powers of the 5*H* and 6*H* phases are similar, i.e., they increase gradually with decreasing temperature and exhibit a broad maximum around 50–60 K as shown in Fig. 4(b). An inflection point near 50 K in the 5*H* phase appears to correlate with the ferromagnetic transition. However, the magnitude of $S(T)$, especially the enhancement at low temperatures in the 6*H* phase, is much larger than that of the 5*H* phase. The 6*H* phase has a smaller resistivity, but a much higher $S(T)$ than that of the 5*H* phase. The NFL behavior of the $\rho(T)$ at low temperatures indicates that the 6*H* phase may be located at a QCP at the boundary between a ferromagnetic phase and a paramagnetic phase. We can test this possibility by the plot of S/T vs ln T since a linear relationship has been predicted theoretically[20] and observed in other systems[21] close to the QCP. As shown in Fig. 4(c), a linear fit can be made in the plot of S/T vs ln T over a wide temperature range below 90 K in the 6*H* phase, which supports the argument of a QCP. In contrast, the linear fitting is not valid in the S/T vs ln T plot of the 5*H* phase in Fig. 4(c). Since the π^* bandwidth changes in a small step between two neighboring phases in a series of polytype structures, we have fortunately found a QCP, which is normally located only by fine tuning the bandwidth with hydrostatic pressure, magnetic field, and/or chemical substitution. Further measurements of the electrical resistivity and thermoelectric power under high pressure for the 6*H* phase are in progress in order to check whether a Fermi-liquid phase can be restored by broadening the bandwidth. Although we have not yet synthesized the pure 3*C* phase sample, the sample synthesized under 10 GPa includes 5% 3*C* phase. Its thermoelectric power shown in Fig. 4(b) is smaller than that of the 6*H* phase sample. The thermoelectric power is dominated by the most conductive phase in case of multiphase coexistence. A reduced $S(T)$ observed in the sample with 5% 3*C* phase indicates that the 3*C* phase may have an $S(T)$ without the enhancement seen in the 6*H* phase.

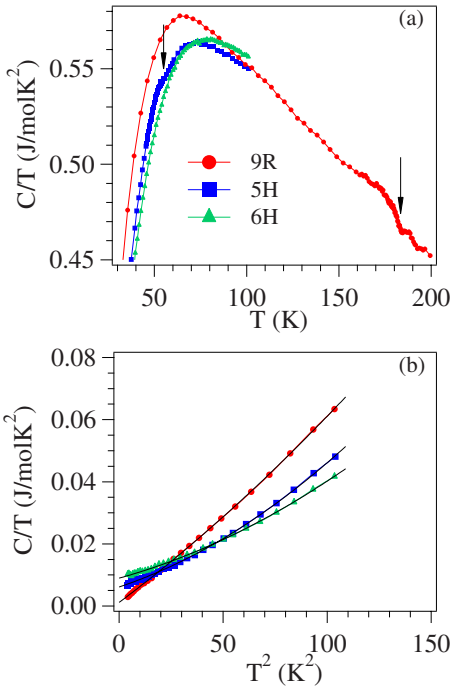

FIG. 6. (Color online) (a) Specific-heat data of the $BaIrO_3$ polytypes showing the anomalies corresponding to the ferromagnetic transitions; (b) the low-temperature specific-heat data in the plot of C/T vs T^2. Solid lines in (b) are the fitting curves.

C. Specific heat

Specific-heat data of these three polytypes are shown in Fig. 6. Weak anomalies can be discerned near T_c in the C_p/T vs T curves of the 9*R* and 5*H* phases. No specific-heat anomaly could be observed down to 2 K in the 6*H* phase. Although the $\chi(T)$, $\rho(T)$, and $S(T)$ curves all exhibit obvious anomalies at T_c, the impact of magnetic ordering on $C_p(T)$ is rather weak in both the 9*R* and the 5*H* phases. A similar anomaly near T_c in the 9*R* phase has been reported in the literature.[22,23] Normally, a sharp λ-shaped anomaly is observed in the $C_p(T)$ near a second-order magnetic transition associated with ordering of localized spins. As in $ZrZn_2$,[24] a weak anomaly in $C_p(T)$ at T_c of the 9*R* and 5*H* phases may signal that band ferromagnetism is taking place.

In order to characterize the contributions from electrons and lattice to the specific heat in these polytypes, we have made a plot of C_p/T vs T^2 and fitted it with the formula

$$C_p(T)/T = \gamma + \beta T^2 + \delta T^4, \quad (1)$$

where the first term describes the electronic contribution and the second and third terms represent the lattice contribution. The Debye temperatures Θ_D can be calculated from β through $\Theta_D = (12\pi^4 nR/5\beta)^{1/3}$, where $n=5$ is the number of atoms in the chemical formula and R is the ideal gas constant. The fitting curves are shown in Fig. 6(b) as the solid lines and the fitting parameters are given in Table I. It was

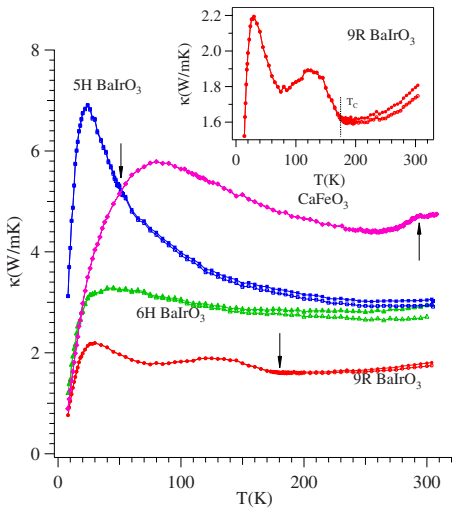

FIG. 7. (Color online) Temperature dependence of the thermal conductivity $\kappa(T)$ of the $BaIrO_3$ polytypes and the perovskite $CaFeO_3$. The $\kappa(T)$ of the $9R$ $BaIrO_3$ is enlarged in the upper inset in order to see clearly the anomaly around T_c. Open symbols represent $\kappa(T)$ after correcting the electronic contribution.

found that Θ_D increases gradually from 268.2 K ($9R$) through 351.9 K ($5H$) to 374.5 K ($6H$) with increasing fraction of corner-shared $IrO_{6/2}$ octahedra. The electronic specific-heat coefficients γ also increase systematically, i.e., 1.15(8), 6.15(6), and 8.99(8) mJ/mol K^2 for $9R$, $5H$, and $6H$, respectively. Since γ is proportional to the density of states at E_F, $N(E_F)$, at low temperatures, the increased γ is consistent with the evolution from an insulator to metals. In contrast, as derived from the high-temperature susceptibility χ_0, the difference of $N(E_F)$ near room temperature between these polytypes is very small. The dramatic change of $N(E_F)$ on crossing T_c is consistent with a gap opening due to the formation of a CDW below T_c,[2,5] which is also supported by measurements of $\rho(T)$ and $S(T)$. At this point, it is interesting to estimate the Sommerfeld-Wilson ratio R_w (Ref. 25): $R_w = \frac{\pi^2}{3}(\frac{\kappa_B}{\mu_B})^2\frac{\chi_0}{\gamma}$ for these polytypes. An $R_w=1$ is obtained in a noninteracting electron system. In a strongly correlated system, however, it has been argued that R_w could be as high as 2 at the limit $U/W=\infty$.[25] We were not able to derive χ_0 in the $9R$ and $5H$ phases since they are ferromagnetic at low temperatures where γ is obtained. For the $6H$ phase, the R_w is 2.14(3). Therefore, the $6H$ $BaIrO_3$ is an exchange-enhanced paramagnetic metal as the QCP is approached from the paramagnetic metal side. Whether the relationship $Cp/T \sim \log T$ is fulfilled at even lower temperatures as seen in the $6H$ $SrIrO_3$ (Ref. 18) will be checked in a future experiment.

D. Thermal conductivity and low-temperature structure

Figure 7 shows the thermal conductivity $\kappa(T)$ of three $BaIrO_3$ polytypes and $CaFeO_3$. The phonon thermal conductivities κ_p were obtained by subtracting from the total $\kappa(T)$ the electronic contributions κ_e according to the Wiedemann-Franz law, viz., $\kappa_e = L_0 T/\rho$, where $L_0 = 2.44 \times 10^{-8}$ W Ω K^{-2} is the Lorenz constant. The phonon thermal conductivity follows a roughly $1/T$ law and peaks out at a low temperature depending on the sample's quality. The peak in $\kappa(T)$, or a hump in some cases, moves to higher temperatures in sintered polycrystalline samples. It is clear from Fig. 7 that the $5H$ $BaIrO_3$ sample has larger grains and an improved contact between grains. All other samples show an essentially glassy κ. However, several interesting features can still be observed. For $9R$ $BaIrO_3$, a jump of κ, which can be seen more clearly in the inset of Fig. 7, occurs at T_c. The influence of spin ordering on κ is normally modest relative to the lattice contribution as in the case of the $5H$ phase and other magnets.[26,27] On the other hand, we have shown that the $\kappa(T)$ will undergo a dramatic change at T_c or T_N if the magnetic transition is accompanied by a lattice change as, for example, in the hexagonal $RMnO_3$ ($R=Y$, Ho-Lu) manganites[28] or the perovskite $RTiO_3$.[29] The perovskite $CaFeO_3$ undergoes a charge disproportionation ($Fe^{4+} \rightarrow Fe^{3+} + Fe^{5+}$) transition at $T_{CD} \sim 290$ K.[30] As shown in Fig. 7, a small increase in κ can be seen at T_{CD} in $CaFeO_3$. Therefore, a dramatic increase in κ below T_c in the $9R$ phase supports the scenario of forming a CDW phase below T_c.

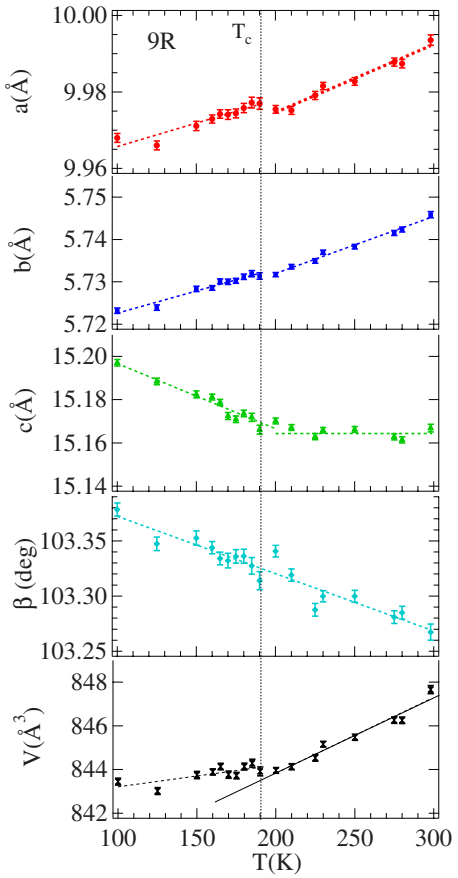

FIG. 8. (Color online) Temperature dependence of the unit cell parameters, a, b, c, β, and V of the $9R$ $BaIrO_3$ from 300 to 100 K. The vertical line marks the ferromagnetism transition temperature T_c. The dashed lines represent the linear fitting to data below and above T_c, yielding the thermal expansion coefficients α.

In order to confirm the structural change crossing T_c, we have measured the low-temperature XRD of the $9R$ $BaIrO_3$ from 300 down to 100 K. The unit cell parameters, a, b, c, β,

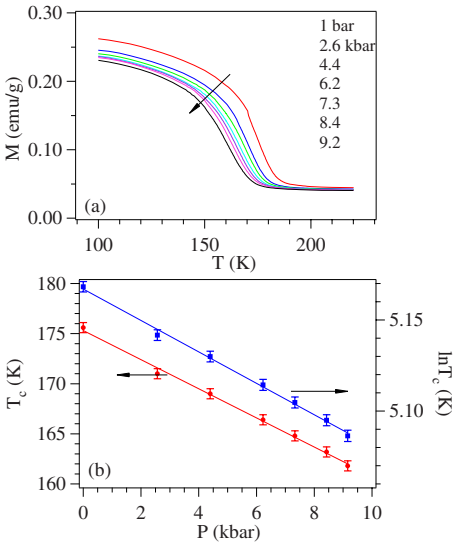

FIG. 9. (Color online) (a) $M(T)$ curves of the $9R$ $BaIrO_3$ under high pressure up to 1 GPa. (b) Pressure dependence of the ferromagnetic transition T_c (left) and $\ln T_c$ (right) as well as the linear fitting curves.

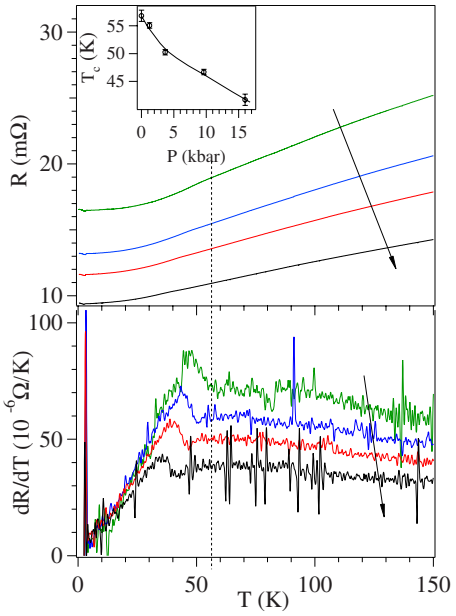

FIG. 10. (Color online) Temperature dependence of the resistance for the $5H$ phase in the temperature range of ferromagnetic transition T_c; inset: pressure dependence of T_c. Arrows in the plot point in the direction of increasing pressure.

and V, as a function of temperature, are shown in Fig. 8. It can be seen that all parameters except β indeed show discontinuous changes near T_c. Because the sensor position relative to the sample is different between the LT-XRD and other measurements of physical properties, T_c obtained from the LT-XRD is slightly higher. The thermal expansion coefficients $\alpha_A \equiv d \ln A/dT$ ($A=a$, b, c, β, and V) were calculated by linear fitting to data below and above T_c and are given in Table I. The most striking change is in α_c, which shows an abrupt drop from $\alpha_c=0$ above T_c to $\alpha_c=-1.9(2)\times10^{-5}$ K^{-1} below T_c. Due to the abnormal thermal contraction of the c axis, the α_V below T_c is much smaller than that above T_c.

E. Pressure effects on the ferromagnetic transitions

There are two reports in the literature about the pressure effect on T_c of the $9R$ $BaIrO_3$.[31,32] Although the resistivity anomaly at T_c has been used to monitor the change of T_c under pressure, quite different pressure coefficients were obtained in the two cases, i.e., −6.1(2) vs −29 K/GPa. The coefficients could be sample dependent. Moreover, the magnitude of the resistivity change at T_c and the definition of T_c from the $\rho(T)$ curve can also alter the dT_c/dP. This issue becomes more complicated in the $9R$ $BaIrO_3$ since there are two close transitions, spin ordering and charge ordering. The magnetization measurement picks up signal from spins, which is the same for polycrystalline[1,31] and single-crystal[2,6] samples. Therefore we have chosen the magnetization measurement under high pressure to study the pressure effect on T_c. The T_c was defined as the minimum of the dM/dT curve for each pressure. It can be seen in Fig. 9 that T_c decreases linearly with increasing pressure, with $dT_c/dP=-14.5(4)$ K/GPa and $d \ln T_c/dP=-0.086(2)$ GPa^{-1}. The pressure coefficient is in the middle between the two values obtained by resistivity measurements,[31,32] but it is still unusually large compared to other known ferromagnetic perovskite oxides such as $BiMnO_3$,[33] $YTiO_3$,[33] $Sr_{1-x}Ba_xRuO_3$,[33] and also $ZrZn_2$.[34] A negative pressure coefficient of T_c has been normally found for both localized-spin and band ferromagnets.

For the $5H$ phase, however, measuring $M(T)$ under high pressure is not feasible because the signal from the Be-Cu pressure chamber is at the same level as that of the sample. Thus, we carried out resistivity measurements under high pressure shown in Fig. 10 to study the pressure effect on T_c. With the same definition of T_c as shown in Fig. 3(b), i.e., a narrow minimum in dR/dT, T_c is suppressed under pressure; but T_c vs P is no longer linear. The initial slope near ambient pressure is much smaller than that in the $9R$ phase. However, without a structural transition at T_c, the suppression of T_c of the $5H$ phase under pressure is much more dramatic than what has been normally seen in ferromagnets, which signals that the ferromagnetic $5H$ phase is near the edge of collapse.

It is interesting to correlate the dramatic change in transport properties observed in the $9R$ vs $5H$ phases with structural and bonding peculiarities of the polytypes.[11] As seen in Fig. 1, the important electron transfer pathway across a shared C stacking in between corner-shared octahedra, which changes critically with bond angle and bond length. In the $5H$ phase, not only is the fraction of C layer stacking increased, which reduces the distance between C layers by 1/3 from that in the $9R$ structure, but also a single perovskite layer is introduced in every four octahedra along the c axis. These structural changes are important to broaden the bandwidth. An insulator to metal transition was not induced in the $9R$ phase under pressure to 12 GPa.[32] Moreover, we have found the Ir-Ir distances within trimers in the $9R$ structure are 2.622 and 2.644 Å. Shrinking the Ir-Ir distance within a trimer takes place at the expense of expanding the important Ir-O-Ir bond length at a C layer. The change in monoclinic distortion between the $9R$ phase and the $5H$ phase results in

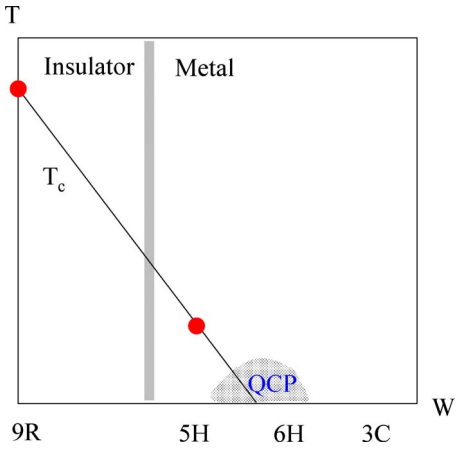

FIG. 11. (Color online) A schematic phase diagram of transition temperature vs bandwidth W of $BaIrO_3$ polytypes. QCP denotes quantum critical point.

a straight Ir-O-Ir bond angle in the 5*H* phase whereas it is bent from 180° in the 9*R* phase. These structural and local bonding changes insure a broader bandwidth in the 5*H* phase than that in the 9*R* phase. A schematic diagram is made in Fig. 11, which organizes all polytype phases of $BaIrO_3$ and their physical properties presented in this paper as a function of their bandwidth.

IV. CONCLUSION

We have made a systematic study of physical properties of three $BaIrO_3$ polytypes, including two new members in the family. With increasing fraction of corner-shared relative to face-shared layer stacking along the *c* axis in the order 9*R* $(hhChhChC) \rightarrow 5H(hChCC) \rightarrow 6H(hCChCC)$, the ground states of $BaIrO_3$ evolve from a ferromagnetic insulator with $T_c \approx 180$ K through a ferromagnetic metal with $T_c \approx 50$ K to an exchange-enhanced paramagnetic metal near a quantum critical point (QCP). All measurements of resistivity, thermoelectric power, thermal conductivity, thermal expansion from the structural study, and the pressure dependence of T_c confirm that the ferromagnetic transition of the 9*R* $BaIrO_3$ is accompanied by a structural change, perhaps forming a CDW phase below T_c. In contrast, the 5*H* $BaIrO_3$ becomes ferromagnetic at a significantly reduced $T_c \approx 50$ K and metallic down to 3.4 K. The highly unusual behavior of $\rho(T)$ near 3.4 K deserves further study. The paramagnetic 6*H* phase remains metallic to 0.05 K. However, the non-Fermi-liquid behavior of the $\rho(T)$ and a much enhanced $S(T)$ at low temperature show a quantum critical point is approached in the 6*H* phase where ferromagnetism is suppressed by bandwidth broadening.

The 6*H* phase has been independently studied by Zhao *et al.*[35] Data from the two groups confirm the magnetic and transport properties of this phase. However, our measurements of thermoelectric power and thermal conductivity and the transport measurement down to 50 mK are critical for a full characterization of this interesting compound. In addition, we have placed the 6H phase in context of a systematic study of all three polytypes, which demonstrates a complete evolution from the ferromagnetic insulator to an exchange-enhanced metal.

ACKNOWLEDGMENTS

We thank the Robert A. Welch Foundation for Grant No. F-1066 and NSF in USA and Grant-in-Aid for Scientific Research (Grant No. 21340092) from the Ministry of Education, Culture, Sports, Science and Technology in Japan for financial support.

*jszhou@mail.utexas.edu

[1] R. Lindsay, W. Strange, B. L. Chamberland, and R. O. Moyer, Jr., Solid State Commun. **86**, 759 (1993).
[2] G. Cao, J. E. Crow, R. P. Guertin, P. F. Henning, C. C. Homes, M. Strongin, D. N. Basov, and E. Lochner, Solid State Commun. **113**, 657 (2000).
[3] M.-H. Whangbo and H.-J. Koo, Solid State Commun. **118**, 491 (2001).
[4] M. L. Brooks, S. J. Blundell, T. Lancaster, W. Hayes, F. L. Pratt, P. P. C. Frampton, and P. D. Battle, Phys. Rev. B **71**, 220411(R) (2005).
[5] K. Maiti, R. S. Singh, V. R. R. Medicherla, S. Rayaprol, and E. V. Sampathkumaran, Phys. Rev. Lett. **95**, 016404 (2005).
[6] T. Nakano and I. Terasaki, Phys. Rev. B **73**, 195106 (2006).
[7] T. Kida, A. Senda, S. Yoshii, M. Hagiwara, T. Takeuchi, T. Nakano, and I. Terasaki, EPL **84**, 27004 (2008).
[8] J. B. Goodenough, J. A. Kafalas, and J. M. Longo, *Preparative Methods in Solid State Chemistry*, edited by P. Hagenmuller (Academic, New York, 1972), pp. 1–69.
[9] C.-Q. Jin, J.-S. Zhou, J. B. Goodenough, Q. Q. Liu, J. G. Zhao, L. X. Yang, Y. Yu, R. C. Yu, T. Katsura, A. Shatskiy, and E. Ito, Proc. Natl. Acad. Sci. U.S.A. **105**, 7115 (2008).
[10] M. Drillon, L. Padel, and J.-C. Bernier, J. Chem. Soc., Faraday Trans. 2 **75**, 1193 (1979).
[11] J.-G. Cheng, J. A. Alonso, E. Suard, J.-S. Zhou, and J. B. Goodenough, J. Am. Chem. Soc. **131**, 7461 (2009).
[12] G. Cao, J. Bolivar, S. McCall, J. E. Crow, and R. P. Guertin, Phys. Rev. B **57**, R11039 (1998).
[13] G. Cao, Y. Xin, C. S. Alexander, J. E. Crow, P. Schlottmann, M. K. Crawford, R. L. Harlow, and W. Marshall, Phys. Rev. B **66**, 214412 (2002).
[14] F. C. Zumsteg and R. D. Parks, Phys. Rev. Lett. **24**, 520 (1970).
[15] R. J. Cava, B. Batlogg, J. J. Krajewski, P. Gammel, H. F. Poulsen, W. F. Peck, Jr., and L. W. Rupp, Jr., Nature (London) **350**, 598 (1991).
[16] J.-S. Zhou, J. B. Goodenough, and B. Dabrowski, Phys. Rev. Lett. **94**, 226602 (2005).
[17] R. P. Smith, M. Sutherland, G. G. Lonzarich, S. S. Saxena, N. Kimura, S. Takashima, M. Nohara, and H. Takagi, Nature (London) **455**, 1220 (2008).

[18] G. Cao, V. Durairaj, S. Chikara, L. E. DeLong, S. Parkin, and P. Schlottmann, Phys. Rev. B **76**, 100402(R) (2007).
[19] J.-G. Cheng, J.-S. Zhou, and J. B. Goodenough (unpublished).
[20] I. Paul and G. Kotliar, Phys. Rev. B **64**, 184414 (2001).
[21] R. Daou, O. Cyr-Choinière, F. Laliberté, D. LeBoeuf, N. Doiron-Leyraud, J.-Q. Yan, J.-S. Zhou, J. B. Goodenough, and L. Taillefer, Phys. Rev. B **79**, 180505(R) (2009).
[22] G. Cao, G. Shaw, and J. W. Brill, J. Phys. IV **12**, Pr9/91 (2002).
[23] N. S. Kini, A. Bentien, S. Ramakrishnan, and C. Geibel, Physica B **359-361**, 1264 (2005).
[24] E. A. Yelland, S. J. C. Yates, O. Taylor, A. Griffiths, S. M. Hayden, and A. Carrington, Phys. Rev. B **72**, 184436 (2005).
[25] K. Wilson, Rev. Mod. Phys. **47**, 773 (1975).
[26] H. Stern, J. Phys. Chem. Solids **26**, 153 (1965).
[27] J. J. Martin and G. S. Dixon, Phys. Status Solidi B **54**, 707 (1972).
[28] J.-S. Zhou, J. B. Goodenough, J. M. Gallardo-Amores, E. Morán, M. A. Alario-Franco, and R. Caudillo, Phys. Rev. B **74**, 014422 (2006).
[29] J.-G. Cheng, Y. Sui, J.-S. Zhou, J. B. Goodenough, and W. H. Su, Phys. Rev. Lett. **101**, 087205 (2008).
[30] M. Takano, S. Nasu, T. Abe, K. Yamamoto, S. Endo, Y. Takeda, and J. B. Goodenough, Phys. Rev. Lett. **67**, 3267 (1991).
[31] J. G. Zhao, L. X. Yang, K. Mydeen, F. Y. Li, R. C. Yu, and C. Q. Jin, Solid State Commun. **148**, 361 (2008).
[32] T. Nakano, Koatsuryoku no Kagaku to Gijutsu **18**, 62 (2008).
[33] J.-G. Cheng, J.-S. Zhou, and J. B. Goodenough (unpublished).
[34] S. Takashima, M. Nohara, H. Ueda, N. Takeshita, C. Terakura, and H. Takagi, J. Phys. Soc. Jpn. **76**, 043704 (2007).
[35] J. Zhao, L. Yang, Y. Yu, F. Li, R. Yu, and C. Jin, Inorg. Chem. **48**, 4290 (2009).